Rev. Roum. Sci. Techn.– Électrotechn. et Énerg.
Vol. **69**, *2*, pp. 195–200, Bucarest, 2024

USING ARTIFICIAL NEURAL NETWORKS TO IMPROVE THE EFFICIENCY OF TRANSFORMERS USED IN WIRELESS POWER TRANSMISSION SYSTEMS FOR DIFFERENT COIL POSITIONS

YILDIRIM ÖZÜPAK[1], EMRAH ASLAN[2]

Keywords: Wireless power transfer; Efficiency; Finite element method; Artificial neural network (ANN).

This study uses magnetic resonance-based coupling theory to study the various placements of transmitter and receiver coils in wireless power transfer (WPT) systems. Various coil placements are examined to show where high efficiency can be achieved within the air gap. Basic characteristics such as self-inductance, mutual inductance, and coupling coefficient were calculated. Artificial neural networks (ANNs) in WPT are a powerful technique for predicting performance characteristics. Using ANNs provides an excellent method for streamlining the design process and reducing time-consuming calculations. To quickly determine and optimize coil design, this study compares recent research on ANN applications in WPT and the performance of different types of ANNs in WPT systems. An artificial neural network (ANN) was trained to predict the magnetic properties of a wireless power transfer (WPT) device. Appropriate cost functions have been implemented to train the ANN properly. It was shown that the trained ANN can effectively reproduce the data obtained by the finite element method (FEM). The results show an effective power transmission at different coil placements, with decreased efficiency observed after a certain distance. These data will help determine the proposed WPT system's air gap and angular limits.

1. **INTRODUCTION**

Wireless power transfer (WPT) is an innovative technology that enables energy transmission without physical connections, revolutionizing the charging and powering of electronic devices. Transferring energy using electromagnetic fields allows users to charge their devices independently of cables and offers practical solutions in many areas of daily life [1,2]. Initiated by Nikola Tesla, this quest has evolved into a multidisciplinary field, with wireless energy transfer serving as a central focus across multiple industries. Nikola Tesla's pioneering work has spurred research into wireless energy transfer, which can be broadly categorized into two main types: near-field and far-field technologies. The earliest efforts in wireless power transmission via electromagnetic radiation were pioneered by Nicola Tesla; however, these efforts experienced setbacks and were discontinued due to the withdrawal of sponsor support [3]. Sahai and Graham continued experimenting with laser-based power transfer but with low efficiency over long distances, primarily applicable in space scenarios. Laser radiation poses hazards despite its potential, with even low-power emissions capable of causing blindness and high-power emissions posing lethal risks due to thermal effects [4].

The efficiency of wireless power transfer (WPT) is significantly influenced by the positional and angular alignment of the transmitter and receiver coils [5–7]. When properly aligned, coils exhibit higher efficiency even at larger air gaps than misaligned coils. A study highlighted in reference [8] focused on estimating the coupling coefficient, emphasizing its critical role in determining efficiency.

The key issue in wireless power transfer (WPT) is maintaining efficient energy transmission at increasing distances between the transmitter and receiver. As the distance increases, the efficiency of power transfer decreases. Researchers have investigated various ways to overcome this issue, including altering coil designs, combining numerous resonators, adjusting impedance matching, and using other approaches. However, due to the many factors impacting power transfer efficiency and the complex interplay between these parameters, determining the ideal values for individual parameters is difficult and time-consuming. As a result, a unique technique for parameter computing for WPT has been proposed, which incorporates artificial neural networks (ANN). This method aims to identify variables and establish improved correlations between parameters. Accordingly, this review delves into the diverse methodologies of ANN applied in WPT and proposes future implementations to augment the overall efficiency of WPT systems.

Early implementations of ANN in WPT, as presented in [9,10], focused on current control for electric vehicle applications using BP. This implementation aimed to stabilize output current during dynamic wireless charging, which required accurate prediction of disturbances to maintain constant output current. Simulation using MATLAB/Simulink demonstrated the effectiveness of BP in stabilizing output current, although hardware validation was lacking [10]. Subsequent research efforts further explored the application of ANN in WPT. These studies proposed using BP to maximize power transfer through impedance-matching techniques and adaptive filtering. BP algorithms have been simulated to identify optimal frequency matches between transmitter and receiver coils, and practical prototypes have been tested to evaluate power transfer efficiency under varying conditions of distance and misalignment [11]. In addition, PSO has been used to optimize the transfer efficiency and VA in inductively coupled WPT systems, and promising experimental and simulation results have been obtained [12–15].

The 2016 study addressed frequency splitting and misalignment challenges, focusing on inductively coupled WPT systems for short-range applications [16]. It used lumped impedance over different frequencies and transmission efficiency coefficients. Various ANN methods, such as GA and PSO, aided in optimization, reducing frequency splitting and accelerating parameter prediction. In dynamic charging scenarios, such as electric vehicles or biomedical devices, lateral misalignment (LTM) issues have been addressed by predicting and correcting coil misalignment using the BP

[1,2] Dicle Üniversitesi Rektörlüğü, 21280 Sur/Diyarbakir, Türkiye. Emails: yildirim.ozupak@dicle.edu.tr, emrah.aslan@dicle.edu.tr

DOI: 10.59277/RRST-EE.2024.69.2.13

algorithm [17]. Predicting LTM dynamics could mitigate misalignment's adverse effects during dynamic charging scenarios. In addition, researchers explored coil design prediction and improvement through ANN algorithms, using PSO to optimize wire distribution and electromagnetic configurations for concentric circular coils [18]. multi-objective hidden point PSO (MOHPSO) and multi-objective real number PSO (MORPSO) were applied to improve coupler efficiency and streamline design processes, supported by validated results from prototype evaluations. In addition, BP and PSO algorithms were used to fine-tune various parameters when exploring the integration of ANN in WPT converters and fault diagnosis [19,20]. Researchers used BP and PSO methods in their investigations to improve system performance and address issues related to battery degradation and lifetime concerns [21–23].

This study investigates the effectiveness of transformer configurations designed for wireless power transmission (WPT) at different locations and airgap spacings. Various parameters such as mutual inductance (M), coupling coefficient (k), and efficiency are calculated for different positions of the models and varying air gap lengths. The equivalent circuits and coils of the magnetic resonance coupling system are derived using several tools within the ANSYS software suite. A transient analysis of the WPT system is then performed considering different states of transmit and receive coil positions. Optimal estimates for k, M, and efficiency are then determined based on the distance using the ANN algorithm and machine learning (ML), followed by a comparative analysis of the results.

2. MATERIAL AND METHOD

This study section describes the fundamental operation of the analogous circuit utilized in the simulation. Figure 1 shows the WPT system's fundamental equivalent circuit. This circuit will allow analytical calculations of input impedance, transmitted power, and efficiency.

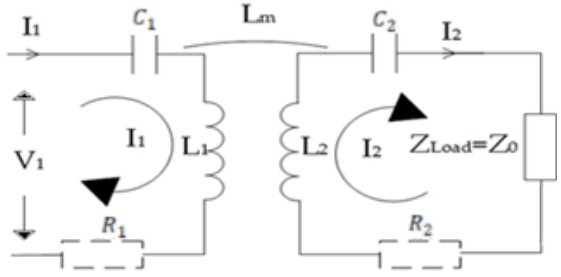

Fig. 1 – Circuit of WPT (wireless power transfer) system.

In this similar circuit, I_1 input current, I_2 output current (receiver current), and V_1 input voltage. The internal resistances within the transmitting and receiving systems encompass various components, including the resonant capacitors C transmit and receive, transmit coil inductance L_1, receive coil inductance L_2, and counter inductance L_{m}, alongside the load impedance Z_{load}. Equation (1) delineates the perimeter equation for the transmitter component, while Equation (2) illustrates the perimeter equation for the receiver component.

$$V_1 = I_1\left(R_1 + \mathrm{j}\omega L_1 + \frac{1}{\mathrm{j}\omega C_1}\right) - I_2(\mathrm{j}\omega L_m), \quad (1)$$

$$0 = I_2\left(R_2 + Z_0 + \mathrm{j}\omega L_2 + \frac{1}{\mathrm{j}\omega C_2}\right) - I_1(\mathrm{j}\omega L_m). \quad (2)$$

Equations (1) and (2) are used to calculate the interaction of currents running between the receiver and transmitter coils, which is shown in Equation (3).

$$I_2 = I_1\left(\frac{\mathrm{j}\omega L_m}{\mathrm{j}\omega L_2 + \frac{1}{\mathrm{j}\omega C_2} + R_2 + Z_0}\right), \quad (3)$$

When eq. (1) is inserted into eq. (3), then the resulting voltage equation is divided by the input current, and the equivalent impedance, also known as the input impedance, is derived, as demonstrated in eq. (4).

$$Z_{eq} = R_1 + \frac{1}{\mathrm{j}\omega C_1} + \mathrm{j}\omega L_1 + (\omega L_m)^2 \times \left(\times \mathrm{j}\omega L_2 + \frac{1}{\mathrm{j}\omega C_2} + + Z_0 + R_2\right)^{-1}. \quad (4)$$

An alternative representation of the equivalent circuit shown in Fig. 1 is the equivalent circuit, as depicted in Fig. 2. The system's efficiency is expressed by eq. (5).

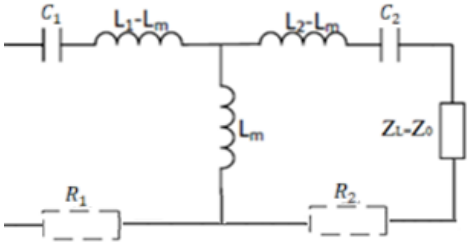

Fig. 2 – Equivalent transfer system.

$$\eta = \frac{P_o}{Pi} = \frac{I_o^2 Z_o}{I_i^2 Z_i}. \quad (5)$$

In this equation, the current I_o represents the current through the receiver I_2, the input current represents the current through the emitter I_1, and the impedance Z_o corresponds to the Z_{load} impedance. Expressing eq. (3) as the ratio of output current to input current yields,

$$\frac{I_{out}}{I_{in}} = \frac{\mathrm{j}\omega L_m}{\mathrm{j}\omega L_2 + \frac{1}{\mathrm{j}\omega C_2} + R_2 + Z_o}. \quad (6)$$

2.1. NEURAL NETWORK STRUCTURE AND TRAINING

This section explores the generation of training data, the partitioning of data into training and testing sets, the creation of the ANN, the training methodology, and the development of cost functions. Each 48,384 geometries inputs nine unique independent variables into the ANN, resulting in 4,418 variables describing magnetic field properties. Subsequently, 49,013 geometries are simulated using a FEM solver, covering various combinations of independent variables and generating 4,418 dependent variables for each geometry.

2.2. DATA GENERATION AND TRAINING/TESTING SETS

Overfitting presents a challenge in artificial neural networks (ANNs), where the network may excel in fitting the data it was trained on but struggles to accurately predict new data points. This issue is particularly pronounced in larger ANNs, although they possess the capacity to approximate more complex functions. The dataset is typically divided into training and test sets to address the risk of overfitting or at least monitor its occurrence. While the ANN learns from the training set, it remains independent from the test set, ensuring that its performance on unseen data points reflects its generalization ability. In this study, every 13th geometry

was assigned to the testing set, ensuring comprehensive coverage of various variables such as air gaps and coil widths. Notably, the ANN underwent training solely with data from the training set, thereby avoiding any influence from the testing set.

2.3. NEURAL NETWORK STRUCTURE

The artificial neural network (ANN) structure comprises four distinct neural networks or branches, each employing identical nine input variables. PyTorch was utilized for constructing the ANN. Figure 3 displays the diverse layering used to simulate individual attributes. The Rectified Linear Unit (ReLu) activation function is mathematically defined on a vector x as follows:

$$R(x) = \begin{cases} x, & x > 0, \\ 0, & x \leq 0. \end{cases} \tag{7}$$

Notably, optimizing the ANN's performance involved training it to interpret the natural logarithm of the flux density rather than its direct value. This improvement is facilitated by the final layer of the stray field branch, which accommodates negative values, thereby circumventing the ReLu activation function. Furthermore, the inductance values specified in nanohenries should be interpreted in the context of a single turn. As both primary and secondary turns increase, the inductance values rise proportionally to the square of the turns.

2.4. TRAINING ALGORITHM

A gradient descent technique minimizes the cost function and trains the ANN, measuring the deviation between the training data and the ANN's predictions. Specifically, the Adam gradient descent method is applied to adjust the ANN's parameters to match the training data produced by FEM. Training typically involves processing batches of input data, with each full iteration through the training dataset referred to as an epoch, aiming to enhance training efficiency,

$$c_L = \langle (I_o - I_T)^T (I_o - I_T) \rangle. \tag{8}$$

The symbol c_L represents the cost associated with the inductance values. I_o denotes the vector containing the inductance values predicted by ANN, while I_T represents the vector of inductance values determined using FEM. The symbol $\langle \cdot \rangle$ denotes the average cost over the batch of geometries. When incorporating ferrite and copper magnetic field strengths into the ANN training process, relying solely on a basic mean squared error (MSE) cost function proves inadequate. The crucial aspect to consider is not solely the magnetic field intensity but energy dissipation. Ferrite losses commonly increase quadratically with the flux density, whereas copper proximity effect losses exhibit a linear relationship with magnetic flux density. Consequently, the minimized cost function c_F ferrite during ANN training is given by:

$$c_F = \langle (f_o^2 - f_T^2)^T (f_o^2 - f_T^2) \rangle. \tag{9}$$

In this equation, f_o denotes the projected magnetic flux density values from the ANN, while f_T represents the magnetic flux densities calculated using FEM. The symbol $\langle \cdot \rangle$ computes the average cost across every channel or image within a batch of geometries. In both the vehicle and ground configurations, each shape incorporates a channel that signifies both the real and imaginary aspects of the field. Equation (9) essentially outlines the cost function as the MSE of the squared magnetic flux density. Although equation (9) suggests that $f_o = \pm f_T$ is an acceptable solution, the ReLu activation function ensures that $f_o \geq 0$. Consequently, there exists only one optimum solution. Similarly, the copper cost c_{Cu} is expressed as:

$$c_{Cu} = \langle (c_o^2 - c_T^2)^T (c_o^2 - c_T^2) \rangle. \tag{10}$$

In eq. (9) and (10), c_o represents a vector of magnetic field strengths predicted by the ANN, while c_T a vector of field strengths calculated by FEM. These equations demonstrate that the ANN is trained to reduce the MSE between the predicted and calculated energy losses. Evaluating relative accuracy provides an indirect approach to assessing precision. Variations in the number of Ampere-turns in the primary and secondary coils proportionally influence overall inaccuracies when magnetic field strength is depicted on a linear scale. Additionally, because some measurements of stray magnetic field intensity are notably high while others are relatively low, a relative error ensures fairness across all measurements. However, utilizing an MSE cost function on linear data may result in comparable linear errors for points with high and low magnetic field strength but significantly different relative errors. Since stray field strengths are logarithmically scaled, reducing the relative error in field strength amounts to minimizing the logarithmic mean square error. It's crucial to acknowledge that logarithmic values can occasionally be negative. Therefore, the ANN's final layer of the stray field branch cannot pass through the ReLu activation function.

2.5. DESIGN OF RECTANGULAR WPT TRANSFORMER MODEL

The study delves into the design aspect of rectangular WPT transformers employing the ANSYS-Maxwell tool. Figure 3 depicts rectangular coils, illustrating the configuration of the WPT transformers. Table 2 details the specific dimensions of the rectangular transformer model.

Table 2
Dimensions of rectangular WPT transformer

Parameter	Receiver coil	Transmitter coil
Turn Number	24	42
Material thickness	2 mm	2 mm
Coil dimension	(395x395) mm	(395x395) mm
Core dimension	(398x398) mm	(398x398) mm

This configuration utilizes the circular transformer model's identical primary and secondary winding counts. A magnetic resonance-coupled WPT system has been developed to accommodate aligned and unaligned conditions across air gap distances. The diverse arrangements of the transmitter and receiver coils, constructed using the ANSYS-Maxwell-3D tool, are illustrated in Fig. 3.

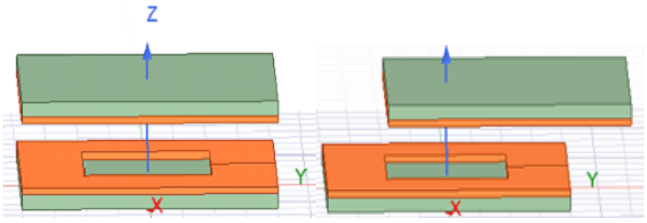

Fig. 3 – Illustrates the aligned receiver and transmitter WPT models.

3. **RESULT DISCUSSION**

3.1. ARTIFICIAL NEURAL NETWORK RESULTS

This section examines the efficiency of the ANN across four primary functions. Unless explicitly stated otherwise, all performance metrics are assessed using the test rather than the training set. Notably, the ANN demonstrated remarkable accuracy in forecasting inductance values. The R2 value, a reliable gauge of the neural network's precision, consistently maintained a high level across all inductance measurements following 1250 training epochs. Figure 4 vividly portrays the proficiency of the ANN in acquiring knowledge of inductances, showcasing a notable convergence between the values calculated by FEM and those predicted by the ANN.

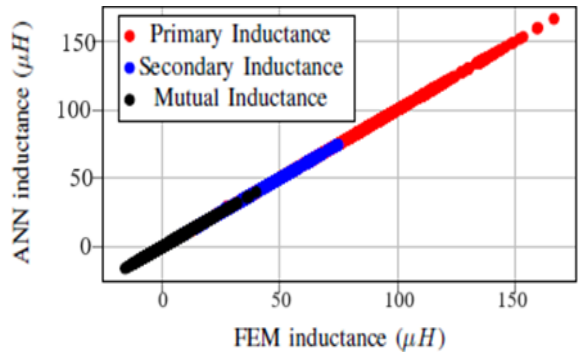

Fig. 4 – Comparative analysis of ANN) and FEM values.

Excitation scenarios involving two amperes-turns for both primary and secondary coils were employed to evaluate the predictive capability of the ANN)in forecasting stray magnetic fields. Subsequently, the magnetic fields generated by the ANN and those produced by FEM were compared for each geometry across various planes.

Two criteria were utilized to validate the efficacy of the ANN: the R2 value, which correlates the MSE with the total energy, and the pass rate, indicating the proportion of the ANN-derived peak field strength falling within a specific margin of the FEM-derived peak field strength. Both criteria are illustrated in Fig. 5, emphasizing that they are solely based on field strength without undergoing logarithmic transformation.

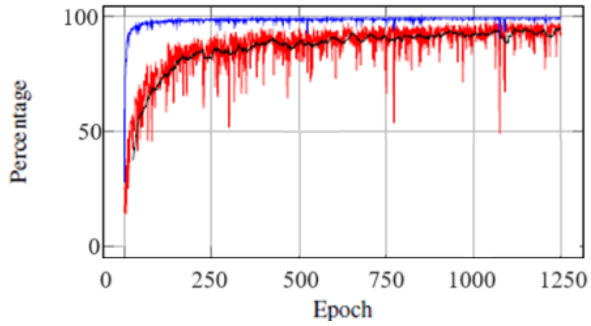

Fig. 5 – Metrics of the effectiveness of the artificial neural network in representing stray fields.

When assessing the ANN performance in simulating ferrite magnetic fields, we computed an estimated energy loss for each geometry based on data generated by both FEM and ANN. It was postulated that ferrite energy losses correlate directly with the average of the squared flux density. After completing 1250 training epochs, the ANN achieved an R2 of 98.9 %. Similarly, we evaluated the accuracy of the ANN in simulating copper magnetic fields using a comparable method to that of ferrite magnetic fields, comparing the energy losses computed by the ANN with those determined by FEM. Following 1 250 epochs, the ANN attained an R2 value of 99.1 %. Figure 6 demonstrates the improvements in ANN performance observed during training for both copper and magnetic field parameters.

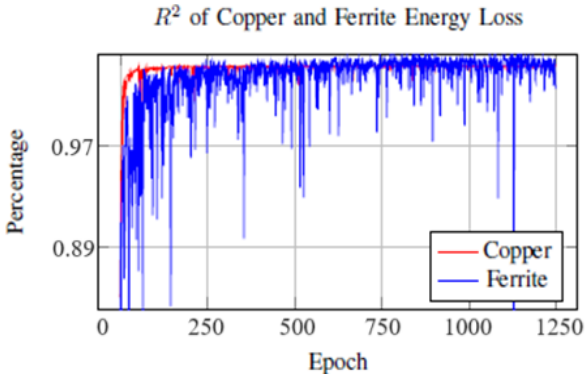

Fig. 6 – Predictive capability enhancement for magnetic field losses throughout the training phase.

3.2. FINITE ELEMENT METHOD ANALYSIS OF ALIGNED TRANSFORMERS

The results obtained from the simulations for the models are displayed in Table 3. Changes in the distance of the air gap between the coils and the relocation of the models have a more significant effect on mutual inductance (*M*) than the coils' self-inductance. In scenarios where positions vary, reducing the air gap distance between the transmit and receive coils led to an elevation in both the mutual inductance (*M*) and the coupling coefficient (*k*).

Table 3

Analysis results of aligned coils of WPT transformer

Distance	Coupling coefficient (k)	Transmitter coil inductanc (L_p[μH])	Receiver coil inductance (L_s[μH])	Mutual inductance (M [μH])	Efficiency (%)
0 cm	0.473	151.615	50.205	39.984	89.5
5 cm	0.273	141.169	47.415	19.991	60.1
10 cm	0.179	139.899	44.114	14.123	30.9

The assessment outcomes concerning the aligned coils of the WPT transformer offer pivotal insights into the system's operational performance. With the coils precisely aligned, it becomes feasible to accurately gauge the efficacy of power transfer and the overall functionality of the transformer. These assessment findings serve as a cornerstone for further enhancements and refinements in WPT technology, facilitating the development of more effective and sustainable energy transfer solutions. An illustrative calculation was also conducted using the developed algorithm, showcasing the derived values for *k*, *M*, and efficiency in the case of aligned coils. Corresponding calculated values for alternative scenarios are delineated in Table 4 and Table 6.

Table 4

k, *M* and efficiency to aligned state

		0	5	10
k	ANSYS-Maxwell	0.473	0.273	0.179
	ANN-Results	0.489	0.281	0.192
M (μH)	ANSYS-Maxwell	39.984	19.991	14.123
	ANN-Results	40.434	21.996	15.158
Efficiency (%)	ANSYS-Maxwell	89.5	60.1	30.9
	ANN-Results	90.3	61.8	31.9

This table compares the results obtained using two methods, ANSYS simulation and ANN, for various parameters such as inductance and efficiency. In the first section, the inductance values for each coil are presented. While slight differences exist between the results obtained from ANSYS and ANN, both methods provide similar inductance values overall. Moving to the second section, the efficiency percentages are provided. Once again, we observe similarities between the results obtained from ANSYS and ANN. This suggests that the ANN approach performs comparably to ANSYS simulation in accurately predicting both inductance and efficiency values. Overall, the table indicates that the ANN method yields results closely aligned with those obtained from ANSYS simulation, demonstrating its effectiveness in accurately estimating inductance and efficiency parameters for the coils.

3.3. ANALYSIS OF UNALIGNED TRANSFORMERS

This part of the research examines the unaligned configurations of different transformer models intended for the WPT system. The outcomes derived from these investigations are showcased in Tables 5 and 6. The misalignment occurs on the horizontal axis. The alignment is in cm in length and occurs gradually in 1 cm steps.

Table 5

Analysis results of unaligned coils of WPT transformer

Distance	Coupling coefficient (k)	Transmitter coil inductance (L_p[μH])	Receiver coil inductance (L_s [μH])	Mutual inductance (M[μH])	Efficiency (%)
0 cm	0.551	149.056	48.941	39.007	88.1
5 cm	0.401	149.854	48.932	34.021	59.1
10 cm	0.325	150.952	48.456	27.155	31.2

Table 6

k, *M*, and efficiency to unaligned coils

		0	5	10
k	ANSYS-Maxwell	0.551	0.401	0.325
	ANN-Results	0.556	0.408	0.341
M	ANSYS-Maxwell	39.007	34.021	27.155
	ANN-Results	40.013	34.246	27.504
Efficiency (%)	ANSYS-Maxwell	88.1	59.1	31.2
	ANN-Results	89.6	60.4	32.2

Table 6 presents the calculated k values, M, and efficiency for unaligned coils obtained from ANSYS simulations and ANN results. For *k*, the values obtained from the ANN results are slightly higher across all cases than those from ANSYS simulations, indicating a slightly stronger coupling between the coils as predicted by the artificial neural network model. Similarly, for *M*, the values from the ANN results show a slight increase compared to ANSYS simulations. This suggests that the ANN model predicts a slightly higher mutual inductance between the coils in the unaligned configuration. Regarding efficiency, both ANSYS simulations and ANN results show an improvement in efficiency compared to the aligned coil configuration. The ANN results exhibit slightly higher efficiency values across all cases than ANSYS simulations, indicating that the artificial neural network model predicts slightly better efficiency in unaligned coil configurations. Overall, the table demonstrates the effectiveness of the artificial neural network approach in predicting coupling coefficient, mutual inductance, and efficiency for unaligned coil configurations, with results closely matching those obtained from ANSYS simulations.

4. CONCLUSION

Wireless power transfer (WPT) technology is rapidly advancing with the increasing demand for applications like mobile phones and electric cars. However, several challenges hinder its effectiveness, including coil design, impedance matching, resonant frequency, and alignment, all of which impact power transfer efficiency. Soft computing offers a solution by providing quick estimates and reliable accuracy for optimizing WPT variables and improving other parameters, ultimately maximizing power transfer efficiency. Artificial neural networks (ANN) for WPT optimization streamline complexity and identify optimal parameters for increased efficiency. Although still in its early stages, ANN's adaptability and predictability offer straightforward solutions to complex WPT problems. This study examines the impact of aligned and unaligned transformer models on WPT system efficiency. In unaligned scenarios, efficiency decreases significantly due to low mutual common inductance. However, effective wireless energy transfer is achievable up to certain air gap values in the unaligned scenario. Efficiency values are computed using ANSYS-Maxwell-3D, considering skin effect and proximity effect in transmitter and receiver coils. ANNs demonstrate high accuracy in approximating FEM data, even for untrained coil geometries. However, ANN performance is lowest in predicting stray fields, likely due to the wide range of magnetic field strength observations and required field measurements for each coil configuration. While a more robust ANN could potentially improve performance, its effectiveness is ultimately constrained by FEM data tolerance limits.

Received on 23 September 2023

REFERENCES

1. N. Tesla, *Art of Transmitting Electrical Energy through Natural Mediums*, U.S. Patent No. 787, 412 (1905).
2. W.C. Brown, *Experimental Airborne Microwave Supported Platform*, Raytheon Co Burlington, MA Microwave and Power Tube Div. (1965).
3. A. Sahai, D. Graham, *Optical wireless power transmission at long wavelengths*, IEEE Int. Conf. on Space Optical Sys & App. (ICSOS), pp. 164–170 (2001).
4. T. Bouanou, H. El Fadil, A. Lassioui, I. Bentalhik, M. Koundi, S. El Jeilani, *Design methodology and circuit analysis of wireless power transfer systems applied to electric vehicles wireless chargers*, World Electr. Veh. J., **14**, p. 117 (2023).
5. Z. Yi, M. Li, B. Muneer, Q. Zhu, *High-efficiency mid-range inductive power transfer employing alternative-winding coils*, IEEE Trans. Power Electron., **34**, *7*, pp. 6706–6721 (2019).
6. Y. Yamada, T. Imura, *An efficiency optimization method of static wireless power transfer coreless coils for electric vehicles in the 85 kHz band using numerical analysis*, IEEJ Trans. Electr. Electron. Eng., **17**, *10* (2022).
7. Y. Yamada, K. Sasaki, T. Imura, Y. Hori, *Design method of coils for dynamic wireless power transfer considering average transmission power and installation Rate*, IEEE 6th Southern Power Electronics Conference (SPEC), Kigali, Rwanda. 2021.
8. R. Navid, W. Jun, Y. Xibo, *In-situ measurement and investigation of winding loss in high-frequency cored transformers under large-signal condition*, IEEE Open J. Ind. Appl., **3** (2022).
9. L. Feng, L. Yanjie, Z. Siqi, C. Yifang, S. Xuan, D. Yutong, *Wireless power transfer tuning model of electric vehicles with pavement materials as transmission media for energy conservation*, Appl. Energy, **323**, p. 119631 (2022).
10. V. Jiwariyavej, T. Imura, Y. Hori, *Coupling coefficients estimation of wireless power transfer system via magnetic resonance coupling using information from either side of the system*, IEEE J. Emerg. Sel. Top. Power Electron., **3**, *1*, pp. 191–200 (2015).

11. J. Tian, A. P. Hu, *Stabilising the output voltage of wireless power pickup through parallel tuned dc-voltage controlled variable capacitor*, Electron. Lett., **52**, *9*, pp. 758–759 (2015).
12. Y. Tian, Y. Sun, Y. Su, Z. Wang, C. Tang, *Neural network-based constant current centered of dynamic wireless power supply system for electric vehicles*, Inf. Technol. J., **11**, *7*, pp. 876–883 (2012).
13. K. G. El-Sayed, R. Al Ahdab, A. El-Shenawy, *Neural network frequency selector for maximum power transfer*, Int. J. Inf. Electr. Eng., **5**, *5*, p. 342 (2015).
14. K. G. ElSayed, N.A. Elessawy, A.K. ElShenawy, *Wireless power transfer system modelling based on neural network with adaptive filtering*, International Conference: High Performance Computing & Simulation (HPCS), 2015.
15. N. Hasan, T. Yilmaz, R. Zane, Z. Pantic, *Multi-objective particle swarm optimization applied to the design of wireless power transfer systems*, IEEE Wireless Power Transfer Conference (WPTC), 2015.
16. M. Wang, J. Feng, Y. Shi, M. Shen, J. Jing, *A novel PSO-based transfer efficiency optimisation algorithm for wireless power transfer*, Prog. Electromagn. Res., C, **85**, pp. 63–75 (2018).
17. Q.Z. Wang, *Optimisation of multiresonant wireless power transfer network based on generalised coupled matrix*, Hindawi Math. Prob. Eng., p. 6803530, 2017.
18. J. Bito, M. Tentzeris, *A real-time electrically controlled active matching circuit utilising genetic algorithm for wireless power transfer to biomedical implants*, IEEE Trans. Microw. Theory Tech., **64**, *2*, pp. 365–374 (2016).
19. R. Narayanamoorthi, A.V. Juliet, G. Santhoshkumar, K. Selvakumar, *Frequency split elimination of short-range wireless power transfer system by active matching tuning circuit*, Indian J. Sci. Technol., **9**, *42*, p. 101842 (2016).
20. A. Dominic, R. Narayanamoorthi, A. Vimala, *PSO based matching circuit tuning system for magnetic resonance based wireless power transfer in biomedical implants*, J. Control Theory Appl., **9**, *16*, pp. 8153–8158 (2016).
21. R. Tavakoli, Z. Pantic, *ANN-based algorithm for estimation and compensation of lateral misalignment in dynamic wireless power transfer systems for EV charging*, IEEE Energy Conversion Congress and Exposition (ECCE), 2017.
22. A. Marinescu, M. Morega, Exposure of active medical implants bearers to electromagnetic emissions from wireless power transfer systems, Rev. Roum. Sci. Techn. – Électrotechn. et Énerg., **67**, *2*, pp. 213–218 (2022).
23. A. Agçal, A. Kalay, R. Cetin, *Wireless power transfer for underwater vehicles*, Rev. Roum. Sci. Techn. – Électrotechn. et Énerg., **68**, *2*, pp. 194–199 (2023).